

# Modeling and Control of a Quadrotor UAV with Aerodynamic Concepts

Wei Dong, Guo-Ying Gu, Xiangyang Zhu, Han Ding

**Abstract**—This paper presents preliminary results on modeling and control of a quadrotor UAV. With aerodynamic concepts, a mathematical model is firstly proposed to describe the dynamics of the quadrotor UAV. Parameters of this model are identified by experiments with Matlab Identify Toolbox. A group of PID controllers are then designed based on the developed model. To verify the developed model and controllers, simulations and experiments for altitude control, position control and trajectory tracking are carried out. The results show that the quadrotor UAV well follows the referenced commands, which clearly demonstrates the effectiveness of the proposed approach.

**Keywords**—Quadrotor UAV, Modeling, Control, Aerodynamics, System Identification.

## I. INTRODUCTION

WITH the development of micro-electronic technologies, the quadrotor UAV draws a lot of attention in recent years due to its advantages of compact size, agility and autonomous flight. A mature quadrotor system can be used for reconnaissance, rescue, photography and works that are dangerous or space limited for human beings [1], [2].

Many researchers involve themselves into this area in recent years. As in [3]–[5], Samir Bouabdallah et al. carried out a series of researches on the control system of the quadrotor UAV. In their works, the rigid body dynamics of a quadrotor UAV and several effects of aerodynamics were studied. They implemented several controllers, including the PID controller, backstepping controller, sliding-mode controller, and so on. By comparison, a so called integral backstepping method was proposed [5]. The backstepping controller and sliding-mode controller have great influences on subsequent researchers. E. I. Pounds et al. presented a delicate method to identify the rigid body dynamics of the quadrotor UAV and an attitude control algorithm was adopted by root locus analysis [6]. In [7], a PD controller was presented by V. Kumar et al., and performs well in their robotic team [8].

From the brief review, although the rigid body dynamics and several aerodynamic effects have been analyzed by Bouabdallah et al. [3], [5], a complete dynamic model, especially that can be adopted for position control, is still missing.

For this reason, to develop a dynamic model that can fully describe the quadrotor UAV is necessary. Such model can greatly help researchers to design controllers in an analytical way and predict the behaviors of the quadrotor UAV via

simulation. In this paper, we aim to obtain this kind of model for a special case, which is under the assumptions that the quadrotor is well controlled at a fixed height and the angle of attack is small. We focus on studying the dynamics of rate loop and speed loop. By the linear estimation and identification, a parameterized transfer function for a selected quadrotor platform is obtained. A group of PID controllers are then designed by the root locus analysis and Ziegler-Nichols tuning rules based on the developed model. Finally, simulations and experiments are carried out to verify the model and the control strategy.

The remainder of this paper is organized as follows. Section II gives a brief introduction to the experimental platform. The model is derived in Section III, and the controller is designed in Section IV. Then the results are shown in Section V, and Section VI concludes this work.

## II. QUADROTOR PLATFORM

A so called Hummingbird quadrotor is chosen from Ascending Technologies, GmbH, which has a mature hardware system and sufficient software packages. With SDK, control algorithms can be easily simulated in Matlab Simulink and converted to embedded codes with no gap. The two level processors structure and safe landing mode can protect the quadrotor from damages in most cases. For these reasons, many researchers choose it as their experimental platform [7], [9], [10].

This platform is shown in Fig. 1. The tip-to-tip wingspan is 50cm and the height is 8cm. It weighs 500g with a capability of additional 200g payload. The attitude is sensed by three gyroscopes along with a 3D magnetometer. And three accelerometers are equipped in the system to measure the acceleration in body fixed coordinates. The height is sensed by a pressure sensor. The speed and position information come from a GPS unit. All of these characteristics provide enough hardware basis for outdoor experiments.

## III. MODELING

In order to derive a complete dynamic model, the rigid body dynamics, motor dynamics and the effects of aerodynamics are studied in this section.

### A. Rigid body dynamics

Rigid body dynamics of the quadrotor UAV governs the response of attitude control. The expressions are derived in two coordinate systems: an inertial coordinates and a body fixed coordinates.

Wei Dong, Guo-Ying Gu, Xiangyang Zhu and Han Ding are with the State Key Laboratory of Mechanical System and Vibration, School of Mechanical Engineering, Shanghai Jiao Tong University, Shanghai 200240, China; email:chengquess@sjtu.edu.cn, guguoying@sjtu.edu.cn, mexyzhu@sjtu.edu.cn, hding@sjtu.edu.cn

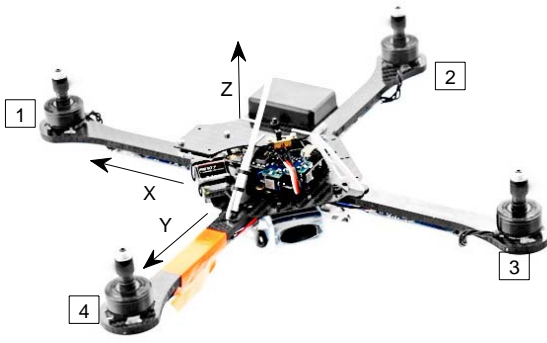


Fig. 1. Hummingbird quadrotor

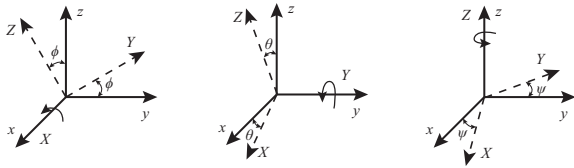


Fig. 2. Attitude definition

The body fixed coordinates is defined as follows. As indicated in Fig. 1, the lever marked with orange strip is chosen as the Y axis, and the perpendicular lever is the X axis. Then the Z axis is defined by the right hand rule.

For inertial coordinates, the point where the quadrotor starts its flight is set as the origin, and an east-north-up orthogonal coordinate system is established by the right hand rule.

With attitude angles defined as in Fig. 2, the transformation matrix from inertial coordinates to body fixed coordinates is

$$R(\phi, \theta, \psi) = \begin{bmatrix} c\psi c\theta & c\psi s\theta s\phi - s\psi c\phi & c\psi s\theta c\phi + s\psi s\phi \\ s\psi c\theta & s\psi s\theta s\phi + c\psi c\phi & s\psi s\theta c\phi - s\psi s\phi \\ -s\theta & c\theta s\phi & c\theta c\phi \end{bmatrix} \quad (1)$$

where  $s$  stands for sin,  $c$  stands for cos, and  $\phi$ ,  $\theta$ ,  $\psi$  represent attitude angles of roll, pitch, yaw respectively.

In the body fixed coordinates, the direct inputs are RPM (revolutions per minute) commands for the motors. The resultant outputs are Z directional thrusts in body fixed coordinates. However, the concerned outputs are attitude and position. To eliminate this gap, four control variables are defined as

$$\begin{cases} U_1 = F_1 + F_2 + F_3 + F_4 \\ U_2 = (F_3 - F_1)L \\ U_3 = (F_2 - F_4)L \\ U_4 = M_1 + M_3 - M_2 - M_4 \end{cases} \quad (2)$$

where  $F_1$ ,  $F_2$ ,  $F_3$  and  $F_4$  are thrusts,  $M_1$ ,  $M_2$ ,  $M_3$  and  $M_4$  are momentums, and  $L$  is the lever length as illustrated in Fig. 3. The subscripts correspond to the ordinal numbers in Fig. 1.

According to the Newton-Euler formalism, the rigid body

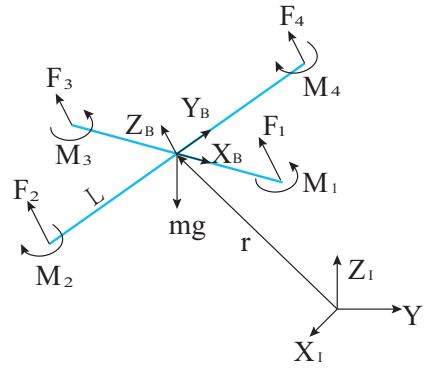


Fig. 3. Force diagram for quadrotor

dynamics is governed by

$$\begin{cases} m\ddot{r} = R \begin{bmatrix} 0 \\ 0 \\ U_1 \end{bmatrix} - \begin{bmatrix} 0 \\ 0 \\ mg \end{bmatrix} - \dot{q} \times m\dot{r} \\ I\ddot{q} = \begin{bmatrix} U_3 \\ U_2 \\ U_4 \end{bmatrix} - \dot{q} \times I\dot{q} \end{cases} \quad (3)$$

where

|     |                            |     |                              |
|-----|----------------------------|-----|------------------------------|
| $m$ | mass of the quadrotor      | $g$ | local gravity constant       |
| $r$ | position in inertial frame | $q$ | attitude in body fixed frame |
| $I$ | rotary inertia             |     |                              |

Since the rotary inertia is small and the quadrotor UAV is symmetric, an estimation for (3) can be expressed in the form of (4), which is also adopted by other researchers [3], [5], [7]

$$\begin{cases} \ddot{x} = U_1(\sin \psi \sin \phi + \cos \psi \sin \theta \cos \phi)/m \\ \ddot{y} = U_1(\sin \psi \sin \theta \cos \phi - \cos \psi \sin \phi)/m \\ \ddot{z} = U_1 \cos \phi \cos \theta / m - g \\ \ddot{\phi} = U_2 / I_{xx} \\ \ddot{\theta} = U_3 / I_{yy} \\ \ddot{\psi} = U_4 / I_{zz} \end{cases} \quad (4)$$

where  $I_{xx}$ ,  $I_{yy}$ ,  $I_{zz}$  are rotary inertia around X, Y, Z axis respectively.

### B. Motor Dynamics

The dynamics of DC motor is generally described as [11], [12]

$$\begin{cases} L_i \frac{di}{dt} + Ri + k_e \omega_m = u \\ J \frac{d\omega_m}{dt} = \tau - \tau_d \end{cases} \quad (5)$$

where

|              |                           |          |                   |
|--------------|---------------------------|----------|-------------------|
| $L_i$ :      | coefficient of inductance | $i$ :    | armature current  |
| $R$ :        | armature resistance       | $k_e$ :  | back emf constant |
| $\omega_m$ : | speed of motor            | $u$ :    | armature voltage  |
| $J$ :        | inertia of motor          | $\tau$ : | torque of motor   |
| $\tau_d$ :   | load                      |          |                   |

### C. Effects of Aerodynamics

Two main effects are taken into consideration. One concerns how thrust is generated while the other deals with the drag force.

The thrust  $T$  produced by each motor is calculated as

$$T = \rho C_T A \omega_m^2 R^2 \quad (6)$$

where

$C_T$ : thrust coefficient     $\rho$ : air density  
 $A$ : rotor disk area         $R$ : blade radius

According to (4) and (6),  $\ddot{\phi}$  and  $\ddot{\theta}$  are related to motors' speeds in the form of

$$\begin{cases} \ddot{\phi} = \rho C_T A R^2 (\omega_3^2 - \omega_1^2) \approx 2\rho C_T A R^2 \omega_1 \delta\omega_\phi \\ \ddot{\theta} = \rho C_T A R^2 (\omega_2^2 - \omega_4^2) \approx 2\rho C_T A R^2 \omega_4 \delta\omega_\theta \end{cases} \quad (7)$$

where  $\omega_1, \omega_2, \omega_3, \omega_4$  are rotary speeds of four rotors,  $\omega_3 = \omega_1 + \delta\omega_\phi$ , and  $\omega_2 = \omega_4 + \delta\omega_\theta$ .

Considering the flight at a fixed height, the aerial drag force is expressed as [13]

$$D = \frac{1}{2} C_D \rho \bar{v}^2 S \quad (8)$$

where

$D$ : drag force                       $C_D$ : drag force coefficient  
 $\bar{v}$ : speed of the quadrotor         $S$ : effective drag area

In order to ensure that the quadrotor UAV flies in a steady speed, (6) should be equal to (8). Thus, one can obtain

$$\rho C_T A \omega_e^2 R^2 \sin \alpha = \frac{1}{2} \rho C_D \bar{v}^2 (S_t \sin \alpha + S_s \cos \alpha) \quad (9)$$

where

$S_t$ : planar area from top view     $\alpha$ : angle of attack  
 $S_s$ : planar area from side view    $\omega_e$ : equivalent motor speed

Furthermore, when a quadrotor flies at a fixed height, the equivalent thrust ( $U_1$ ) itself is a function of the angle of attack according to (4) and (6). Substituting those two equations into (9), the flying speed is a function of the angle of attack as

$$\begin{aligned} \bar{v} &= \sqrt{\frac{2mg \sin \alpha}{\cos \alpha \rho C_D (S_t \sin \alpha + S_s \cos \alpha)}} \\ &\approx \sqrt{\frac{2mg}{\rho C_D}} \sqrt{\frac{\alpha}{S_s} - \frac{S_t \alpha^2}{S_s^2}} \end{aligned} \quad (10)$$

From (10), when  $\alpha$  is small, the side area  $S_s$  dominates the drag effect. However, the influence of  $S_t$  increases when  $\alpha$  becomes larger.

## IV. CONTROLLER DESIGN

Based on the proposed dynamic models (4), (5) and (10), the controllers will be designed in this section.

TABLE I  
IDENTIFICATION RESULTS FOR C(S)

| Item | $K_a$ | $\tau_m$ | Experiment Time(s) |
|------|-------|----------|--------------------|
| 1    | 22.75 | 0.001    | 144                |
|      | 18.00 | 0.001    |                    |
| 2    | 13.05 | 0.001    | 122                |
|      | 17.61 | 0.001    |                    |
| 3    | 17.53 | 0.001    | 72                 |
|      | 18.29 | 0.001    |                    |
| 4    | 15.48 | 0.001    | 62                 |
|      | 15.48 | 0.001    |                    |
| 5    | 25.58 | 0.001    | 65                 |
|      | 16.49 | 0.001    |                    |
| 6    | 13.71 | 0.001    | 72                 |
|      | 32.30 | 0.001    |                    |

### A. Attitude and Position Control

1) *System identification*: The block diagram of this system is shown in Fig. 4, which consists of a rate loop(**R**), an attitude loop(**A**), a speed loop(**S**) and a position loop(**P**).

The identification of those subsystems is processed as follows.

**Rate Loop** According to (7), with the consideration that the changes of  $\omega_1$  and  $\omega_4$  are small considering the large values of themselves in practice,  $\ddot{\phi}$  and  $\ddot{\theta}$  are governed by  $\delta\omega_\phi$  and  $\delta\omega_\theta$  with linear relationship respectively. And from equation (5), the motor is a first order system. Thus, the overall transfer function of **C** is a first order system which is expressed as

$$C(s) = \frac{K_a}{\tau_m s + 1} \quad (11)$$

where  $K_a$  stands for the overall gain of this subsystem and  $\tau_m$  represents the delay. To identify the parameters in (11), six experiments are carried out. With a preliminarily designed controller, the quadrotor flies with a time varied attitude. References and responses for the rate loop are recorded in 50Hz. The data are then processed by Matlab Identify Toolbox. The identified results are shown in Table I. Thus, **C**(s) is estimated as (12) by taking mean values from the results

$$C(s) = \frac{19}{0.001s + 1} \quad (12)$$

**Attitude Loop** The open loop behavior is in the form of integral as shown in Fig. 4, which is also proven by experiments.

**Speed Loop** According to (10), even for a quadrotor flying at a fixed height, the relation between attitude and flying speed is nonlinear. In this work, we only consider a special case which is under the assumptions as follows:

- The height of the quadrotor is well controlled
- The quadrotor flies at a fix height
- The attitude angles are small

Thus, for a certain platform, (10) can be expanded by the Taylor series at any nonzero point. Then a first order system is chosen to give an estimation. Noticing the fact that time delay always exists in the conversion from attitude to speed, the transfer function of **STF** in Fig. 4 is proposed as

$$STF(s) = \frac{K_s}{\tau_s s + 1} e^{-Ls} \quad (13)$$

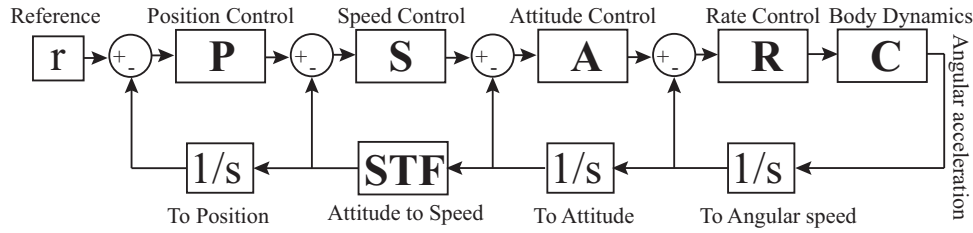


Fig. 4. structure of the control system

 TABLE II  
 IDENTIFICATION RESULTS FOR STF(S)

| Item | $K_s$ | $\tau_s$ | $L$  | Experiment Time(s) |
|------|-------|----------|------|--------------------|
| 1    | 19.61 | 2.69     | 0.47 | 144                |
| 2    | 11.33 | 1.37     | 0.59 |                    |
| 3    | 6.81  | 0.91     | 0.79 | 122                |
|      | 6.66  | 0.81     | 0.81 |                    |
| 4    | 6.13  | 0.63     | 0.84 | 72                 |
|      | 15.50 | 2.12     | 0.57 |                    |
| 5    | 15.50 | 1.92     | 0.58 | 62                 |
|      | 7.47  | 0.77     | 0.81 |                    |
| 6    | 13.63 | 1.84     | 0.65 | 65                 |
|      | 13.07 | 2.17     | 0.83 |                    |
|      | 11.45 | 1.26     | 0.72 | 72                 |
|      | 12.72 | 2.15     | 0.70 |                    |

To identify the parameters, six experiments are also carried out and results are shown in Table II.

Taking mean values from the results and substituting them into (13), STF(s) is estimated as

$$\text{STF}(s) = \frac{11.7}{1.6s + 1} e^{-0.7s} \quad (14)$$

**Position Loop** The open loop behavior is in the form of integral as shown in Fig. 4, which is also proven by experiments.

2) *Control Approach*: With its three-term functionality covering treatment to both transient and steady-state responses, the PID control provides the simplest and yet most efficient solution in many applications. It has been successfully applied for control of the quadrotor [14]. In this work, PID controllers are adopted for those four loops as follows

$$\begin{cases} R = K_{rp} \\ A = K_{ap} \\ S = K_{ps} \left( 1 + \frac{1}{T_{is}s} + T_{ds}s \right) \\ P = K_{pp} \left( 1 + \frac{1}{T_{ip}s} + T_{dp}s \right) \end{cases} \quad (15)$$

where proportional controllers are implemented for **R** and **A** while **S** and **P** are adopted by PID controllers.

Then close loop transfer functions for rate loop( $R_C$ ), attitude loop( $A_C$ ), speed loop( $S_C$ ) and position loop( $P_C$ ) are given as

$$\begin{cases} R_C(s) = \frac{s^2 + 1000s}{s^2 + 1000s + 19000K_{rp}} \\ A_C(s) = \frac{K_{ap}R_C}{s + K_{ap}R_C} \\ S_C(s) = \frac{11.7K_{ps}(T_{ds}s^2 + s + 1/T_{is}s)A_C e^{-0.7s}}{1.6s^2 + s + 11.7K_{ps}(T_{ds}s^2 + s + 1/T_{is}s)A_C e^{-0.7s}} \\ P_C(s) = \frac{K_{pp}(T_{dp}s^2 + s + 1/T_{ip}s)S_C}{s^2 + K_{pp}(T_{dp}s^2 + s + 1/T_{ip}s)S_C} \end{cases} \quad (16)$$

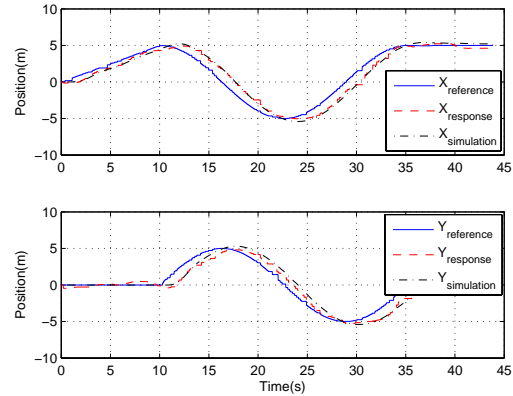


Fig. 5. Comparison between simulation and experiments for position control

For rate and attitude loop, by the root locus analysis, an undamped and fast response system can be obtained when  $K_{rp} = 10$  and  $K_{ap} = 12$  are chosen.

For speed control, the Ziegler-Nichols(Z-N) [11] rules is adopted to tune the parameters. A proportional controller is implemented at the beginning. The critical gain  $K_{cr} = 0.4$  and critical period  $T_{cr} = 2.5$  are obtained. Then PID parameters are selected as  $K_{ps} = 0.24$ ,  $T_{is} = 1.25$  and  $T_{ds} = 0.31$ .

For position loop, the Z-N technique is also adopted, and  $K_{pp} = 0.7$ ,  $T_{ip} = 2.3$ ,  $T_{dp} = 0.28$  are set for the system.

3) *Verification*: In order to verify the analysis, a simulation and a position control experiment implemented with totally same controllers are carried out. Fig. 5 shows the results. Both in experiment and simulation, the controllers follow the references well, which shows the accuracy of the model and the effectiveness of the controllers.

### B. Attitude Control

Similar to the reported controllers in [4] [15], a sliding-mode control algorithm is implemented here.

A linear sliding mode surface is selected as

$$s_1 = c_1 e_1 + e_2 = c_1(z_r - z) + (\dot{z}_r - \dot{z}) \quad (17)$$

where  $z_r$  stands for the reference of altitude,  $z$  is the actual response, and  $c_1$  is a positive number.

A so called exponential reaching law [16] is adopted

$$\dot{s}_1 = c_1(\dot{z}_r - \dot{z}) + (\ddot{z}_r - \ddot{z}) = -\varepsilon_1 \text{sgn}(s_1) - k_1 s_1, \varepsilon_1 > 0, k_1 > 0 \quad (18)$$

where  $\varepsilon_1$  is a small positive number.

Substituting equation (4) into equation (18), one can obtain the control input for altitude control

$$U_1 = \frac{m}{\cos \phi \cos \theta} [c_1(\dot{z}_r - \dot{z}) + \dot{z}_r + \varepsilon_1 \operatorname{sgn}(s_1) + k_1 s_1 + g] \quad (19)$$

## V. EXPERIMENTS

All the experiments are carried out in an outdoor environment. Rate, attitude, speed, position and altitude are controlled by onboard processors running at a frequency of 1000Hz. Trajectory information is sent from a laptop to the position controller at a frequency of 50Hz. The reference and response for each controller are collected to the laptop via a wireless router.

### A. Altitude Control

The results of altitude control are shown in Fig. 6. The subscript *cmd* stands for *command*, *act* stands for *response*, and they keep these meanings through the following text. The steady state error is within 0.5 meter, and the delay is within 7 seconds. Compared with reported controllers [4] [15], it is good enough in the outdoor environment.

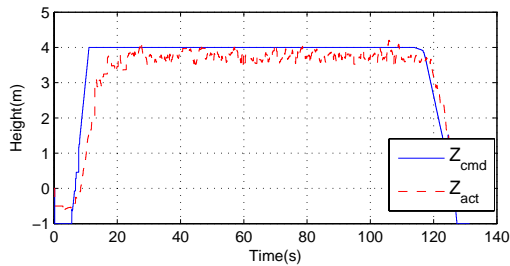


Fig. 6. Results of altitude control

### B. Position Control

The position control is carried out at a fixed flying height of 3 meters. The quadrotor UAV firstly hovers at the position of (0,0,3) for 60 seconds, then it follows several ramp references. The results are shown in Fig. 7. It is satisfactory when compared with the reported results [3], [4], [15]. The steady errors are within 0.5 meter, overshoots are within 15%, and the delays are within 3 seconds. The corresponding results of speed control are shown in Fig. 8, and the results of attitude control are shown in Fig. 9.

In Fig. 8, approximately 1 second delay exists in the speed control. This clearly demonstrates the delay term in (14). The maximum error of 1.4m/s appears at 106s with reference of 5.7m/s in X direction. However, there are no significant influences on the position control at that point.

In Fig. 9, when commands are small ( $\leq 0.2$ rad), which corresponds to the case of hovering with speed less than 1m/s, the maximum error of around 0.1rad arises. This can be explained as follows. On one hand, the controller lacks of integral terms, so it is not sensitive to small errors. On the other hand, disturbances such as wind affect the results.

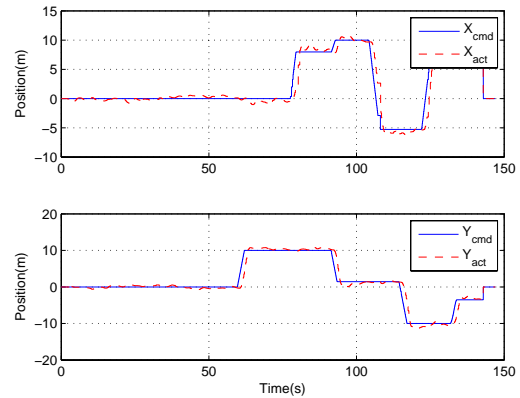


Fig. 7. Results of position control

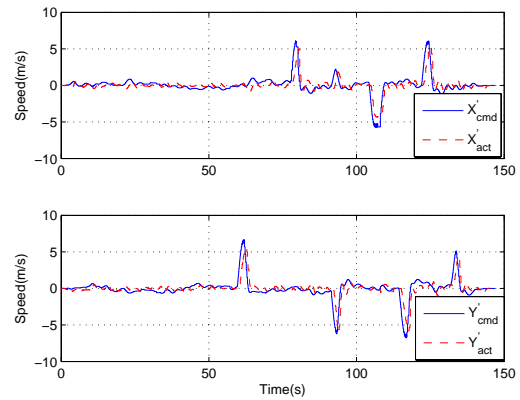


Fig. 8. Results of speed control

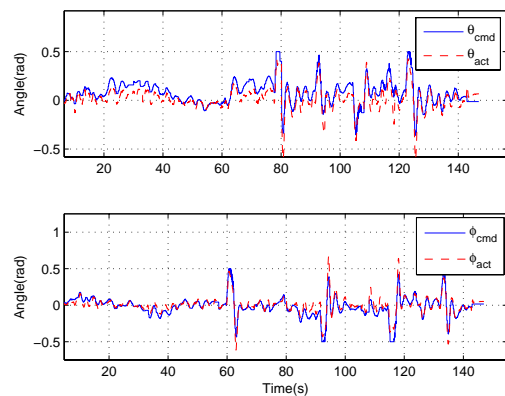


Fig. 9. Results attitude control

The maximum error of 0.1rad(20%) appears in attitude control when the quadrotor accelerates the speed up and the maximum overshoot of 0.25rad(40%) appears in attitude control when the quadrotor decelerates the speed to zero. However, there are no overshoots in speed control at these points due to regulation

of the speed controller as in Fig. 8.

### C. Trajectory tracking

A rectangular trajectory tracking and a circular trajectory tracking are performed. The flying height is 3 meters. Each experiment takes 140 seconds. The results are shown in Fig. 10 and Fig. 11. The trajectory errors are within 0.5 meter.

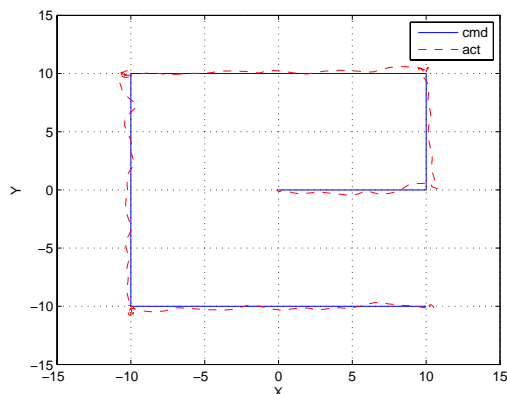


Fig. 10. Rectangular trajectory tracking

## VI. CONCLUSION

In this paper, a complete dynamic model of the quadrotor UAV is proposed for a special case which is under the assumptions that the flight is well controlled at a fixed height and the angle of attack is small. By linear estimation and parameter identification, the transfer function is developed for an off-the-shelf quadrotor UAV. This makes it possible to design controllers in an analytical way. A group of PID controllers are selected and the parameters are tuned according to the developed model. Simulations and outdoor experiments show that the controllers follow the references very well with a maximum error of 0.5 meter in position control and maximum overshoot of 15%. Since the angle of attack is not always small, height is not precisely fixed and random disturbances arise in the outdoor environment, experiments show that the model can be adopted in more general cases than that under the assumptions.

Although only the PID algorithm is selected for analysis, the approach is validated for any other controller. However, the dynamic model is derived from a special case, so more general cases will be studied in future. Another limitation of this work is that the current test is only applied to one quadrotor UAV, and more researches will be taken for different platform in order to generalize the results. Nonetheless, the success of current work will motivate us to move on.

## REFERENCES

[1] V. Kumar and N. Michael, "Opportunities and challenges with autonomous micro aerial vehicles," in *Int. Symp. on Robotics Research*, 2011.

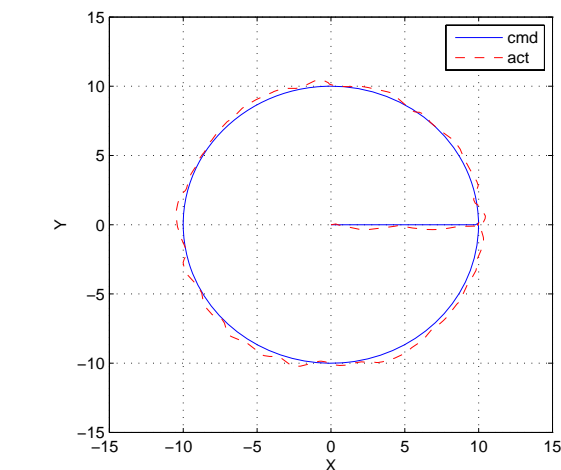


Fig. 11. Circular trajectory tracking

- [2] D. Mellinger, M. Shomin, and V. Kumar, "Control of quadrotors for robust perching and landing," in *International Powered Lift Conference, October 5-7, 2010*, 2010.
- [3] S. Bouabdallah and R. Siegwart, "Full control of a quadrotor," in *Intelligent Robots and Systems, 2007. IROS 2007. IEEE/RSJ International Conference on*. Ieee, 2007, pp. 153–158.
- [4] S. Bouabdallah, R. Siegwart, S. Bouabdallah, and R. Siegwart, "Backstepping and sliding-mode techniques applied to an indoor micro quadrotor," in *Robotics and Automation, 2005. ICRA 2005. Proceedings of the 2005 IEEE International Conference on*. Ieee, 2005, pp. 2247–2252.
- [5] S. Bouabdallah, "Design and control of quadrotors with application to autonomous flying," *Lausanne Polytechnic University*, 2007.
- [6] P. Pounds, R. Mahony, and P. Corke, "Modelling and control of a quadrotor robot," in *Proceedings Australasian Conference on Robotics and Automation 2006*. Australian Robotics and Automation Association Inc., 2006.
- [7] N. Michael, D. Mellinger, Q. Lindsey, and V. Kumar, "The grasp multiple micro-uav testbed," *Robotics & Automation Magazine, IEEE*, vol. 17, no. 3, pp. 56–65, 2010.
- [8] Q. Lindsey, D. Mellinger, and V. Kumar, "Construction of cubic structures with quadrotor teams," *Proc. Robotics: Science & Systems VII*, 2011.
- [9] R. Mahony, V. Kumar, and P. Corke, "Multirotor aerial vehicles: Modeling, estimation, and control of quadrotor," *Robotics & Automation Magazine, IEEE*, vol. 19, pp. 20 – 32, 2012.
- [10] T. Tomic, K. Schmid, P. Lutz, A. Domel, M. Kassecker, E. Mair, I. Grix, F. Ruess, M. Suppa, and D. Burschka, "Toward a fully autonomous uav: Research platform for indoor and outdoor urban search and rescue," *Robotics & Automation Magazine, IEEE*, vol. 19, pp. 57–68, 2012.
- [11] K. Ogata and Y. Yang, *Modern control engineering*. Prentice Hall Upper Saddle River, NJ, USA, 1990, vol. 4.
- [12] S. Bouabdallah and R. Siegwart, "Design and control of a miniature quadrotor," *Advances in Unmanned Aerial Vehicles*, pp. 171–210, 2007.
- [13] J. Leishman, *Principles of helicopter aerodynamics*. Cambridge University Press, 2006.
- [14] A. Salih, M. Moghavvemi, H. Mohamed, and K. Gaeid, "Modelling and pid controller design for a quadrotor unmanned air vehicle," in *Automation Quality and Testing Robotics (AQTR), 2010 IEEE International Conference on*, vol. 1. IEEE, 2010, pp. 1–5.
- [15] R. Xu and U. Ozguner, "Sliding mode control of a quadrotor helicopter," in *Decision and Control, 2006 45th IEEE Conference on*. IEEE, 2006, pp. 4957–4962.
- [16] C. Fallaha, M. Saad, H. Kanaan, and K. Al-Haddad, "Sliding-mode robot control with exponential reaching law," *Industrial Electronics, IEEE Transactions on*, vol. 58, no. 2, pp. 600–610, 2011.